Spatial receptive field structure of double-opponent and simple cells in macaque primary visual cortex

Abhishek De[1,2] & Gregory D. Horwitz[2]

[1]Graduate Program in Neuroscience, [2]Department of Physiology and Biophysics, Washington National Primate Research Center, University of Washington, Seattle, USA

Correspondence: Gregory D. Horwitz, PhD
1959 N.E. Pacific Street
Box 357330, HSB I-714,
Seattle, WA, 98195
Email: ghorwitz@u.washington.edu
Phone: +1-206-616-0565

ABSTRACT

Double-opponent (DO) cells are well-suited to contribute to the spatial processing of color due to their spatially opponent and cone-opponent receptive fields (RFs). However, the representation of visual images by DO cells in monkey primary visual cortex is unclear because the spatial RF structure of DO cells has not been fully characterized. Early reports suggested that DO cells have center-surround RFs, but more recent studies have shown that some DO cells are orientation-tuned. To characterize the RFs of DO cells, we mapped them in awake fixating macaques, fit them with parametric models, and compared them to the benchmark of orientation-tuned simple cells. Neurons were stimulated with colorful, dynamic white noise patterns. Spike-triggered averaging was used to classify each neuron as simple, DO, or neither and to measure its spatial RF. The spatial RF of each neuron was fitted with a Gabor model and a Difference of Gaussians (DoG) model. The Gabor model provided the more accurate description, a result that is incompatible with a center-surround RF organization. The superiority of the Gabor fits was slightly more decisive for simple than for DO cells. A modified (non-concentric) DoG model performed nearly as well as the Gabor model for DO cells.

INTRODUCTION

Double-opponent (DO) cells encode colored edges. They are cone-opponent and thus sensitive to stimulus chromaticity, and they have opposite chromatic preferences in different parts of their receptive field (RF), rendering them sensitive to spatial contrast. These defining characteristics are undisputed, but the spatial structure of DO cells' RFs is controversial.

DO cells in primate primary visual cortex (V1) were originally reported to have a center-surround RF organization, suggesting that they are orientation-untuned (Hubel & Wiesel, 1968; M. S. Livingstone & Hubel, 1984; Michael, 1978; Poggio, 1975). On the other hand, more recent experiments showed that most DO cells are orientation-tuned (Johnson, Hawken, & Shapley, 2001, 2008) but see (Conway, 2001; Conway & Livingstone, 2006). Several factors likely contribute to the difference in findings. For example, one factor is the use of different stimuli that led to different conclusions. Another factor is that most descriptions of DO cell RFs have been either 2-dimensional (2-D) and qualitative or, 1-D and quantitative (e.g. orientation tuning). A complete, quantitative description of DO cell spatial RF structure is not yet available.

Knowing the spatial structure of DO cell RFs is important for understanding their role in image processing. For example, unoriented RFs could contribute to simultaneous color contrast and could be responsible for the well-documented deficiencies in form vision at isoluminance (Gregory, 1977; M. S. Livingstone, & Hubel, D. H., 1987; McIlhagga, 2018; Mullen, 2002). Oriented RFs could contribute to shape-from-shading—the ability to estimate the 3-D shapes of objects from shading cues (Kingdom, 2003; Kunsberg, 2018).

We stimulated every neuron that we isolated with the same white noise stimulus to maintain a constant adaptation state across experiments. We analyzed the data by spike-triggered averaging to identify DO cells and measure their spatial RFs. We fit each spatial RF with two models. The first, the difference of Gaussians (DoG) model, assumes that DO cell RFs are orientation-untuned (Rodieck, 1965). The second, the

Gabor model, assumes that they are orientation-tuned (Jones, 1987; D. L. Ringach, 2002). Both models provide a concise description of RF organization that is useful for image analysis, summarizing data, and making quantitative comparisons between neurons. We compared model fits between DO cells and simple cells—a benchmark cell type that is orientation-tuned (Hubel & Wiesel, 1968; Jones, 1987; Moore IV, 2012; D. L. Ringach, 2002; D. L. Ringach, Shapley, R. M., & Hawken, M. J., 2002).

The Gabor model outperformed the DoG model for most of the simple cells studied, which was expected from previous studies (Jones, 1987; Moore IV, 2012; D. L. Ringach, 2002). Most DO cells were also more accurately described by the Gabor model, which is a novel result. The goodness-of-fit of the Gabor model was similar for simple and DO cells. Some DO cell RFs consisted of a circular center and a crescent-shaped surround, as has been reported previously (Conway, 2001; Conway & Livingstone, 2006). A slight modification of the DoG model captured such RFs and performed nearly as well as the Gabor model for DO cells but poorly for simple cells. Together, these results show that simple and DO RFs are both well-described by the Gabor model, they are poorly described by the DoG model, but the center-crescent surround model is a reasonable description for many DO cells.

METHODS

General

All protocols conformed to the guidelines provided by the US National Institutes of Health and the University of Washington Animal Care and Use Committee. Data were collected from two male and two female rhesus macaques (Macaca mulatta) weighing 7–13 kg. Each monkey was surgically implanted with a titanium headpost and a recording chamber (Crist Instruments) over area V1. Eye position was continuously monitored using either an implanted monocular scleral search coil or an optical eye-tracking system (SMI iView X Hi-Speed Primate, SensoMotoric Instruments).

Monitor calibration

Stimuli were presented on a cathode-ray tube (CRT) monitor (Dell Trinitron Ultrascan P991) with a refresh rate of 75 Hz and background color as uniform gray (x = 0.3, y = 0.3, Y = 43–83 cd/m^2). Monitor calibration routines were adapted from those included in the Matlab Psychophysics toolbox (Brainard, 1997). Emission and voltage-intensity relationships of each monitor phosphor were calibrated using a spectroradiometer (PR650, PhotoResearch). The color resolution of each channel was increased from 8 to 14 bits using a Bits++ video signal processor (Cambridge Research) at the expense of spatial resolution; each pixel was twice as wide as it was tall.

Task

The monkeys sat in a primate chair 0.7–1.0 m from a CRT monitor in a dark room during the experiments. The monkeys were trained to fixate a centrally located dot measuring 0.2 x 0.2° and maintain their gaze within a square 1.0–2.0° fixation window. Successful fixation was rewarded, and fixation breaks aborted trials.

Electrophysiological recordings

We recorded spike waveforms from well-isolated V1 neurons using extracellular tungsten microelectrodes (Frederick Haer, Inc.) that were lowered through dura mater by a hydraulic microdrive (Narishige Inc. or Stoelting Co.). Electrical signals were amplified and digitized at 40 kHz online (Plexon Inc.) and stored in a PC.
After isolating a waveform, we mapped the RF boundaries with oriented bars of different colors based on the modulation of the spiking activity.

Visual stimuli and experimental protocol

Each neuron was stimulated with white noise chromatic checkerboards (Horwitz, Chichilnisky, & Albright, 2005, 2007) . Each stimulus frame was a grid of 10 x 10 pixels, with each pixel subtending 0.2 x 0.2°. The stimulus changed on every screen refresh. The intensity of each phosphor was modulated independently according to a Gaussian distribution with a standard deviation of 5–15% of the physically achievable range. The space-time averaged intensity of each phosphor was equal to its contribution to the background. Neuronal responses to the white noise stimuli were analyzed using spike triggered averaging (**Figure 1A**) (Horwitz et al., 2005).

FIGURE 1 HERE

Cone weights and spatial RF

For each cell, we identified the frame from the spike-triggered averaged stimulus (STA) that differed most from the background, based on the sum of squared red, green, and blue pixel intensities (negative intensities were defined as those below the contribution

to the background). We then took the weighted average of the peak and the two flanking frames (10 pixels x 10 pixels x 3 color channels), reshaped it into a 100 x 3 matrix, and used a singular value decomposition (SVD) to separate this weighted STA into a color weighting function and a spatial weighting function, defined as the first row and column singular vectors, respectively (**Figure 1B**) (Horwitz & Albright, 2005). The color weighting function and the spatial weighting function together captured nearly 65% of the variance in the weighted STA (**Figure 1C–D**). This fraction is biased downward by pixels outside of the RF. Restricting analysis to pixels inside the RF increased the explained variance to 82%.

The color weighting function, which quantifies neuronal sensitivity to modulations of the red, green, and blue phosphors of the display, was converted to cone weights that are assumed to act on cone contrast signals (Weller, 2018). Cone weights were normalized such that the sum of their absolute values was 1 (Derrington, Krauskopf, & Lennie, 1984; Horwitz & Albright, 2005; Johnson, Hawken, & Shapley, 2004). We analyzed only those cells that were spatially opponent (**see Cell Screening**). As a result, each cell had cone weights with different signs in different parts of the RF. There is no principled way of describing such a cell as having cone weights of one sign or the other. Therefore for convenience, we constrained the M-cone weights of all the cells to be positive, and we classified cells as cone-opponent or cone non-opponent by evaluating the signs of L- and S-cone weights relative to the M-cone weight.

Cell screening

We recorded from 401 V1 neurons and omitted 194 from the analyses on the basis of four criteria. Every neuron was required to have an STA with (1) high signal-to-noise ratio (SNR), (2) interpretable structure, (3) spatial opponency, and (4) cone weights that were either clearly opponent or clearly non-opponent. Below, we explain the rationale for each criterion and how they were implemented.

We excluded cells with low signal-to-noise ratio (SNR) because noisy STAs could lead to inaccurate estimates of color and spatial weighting functions. SNR was computed by comparing the peak STA frame to first STA frame and was defined as follows:

$$SNR = \sum_{i=1}^{N} \left(\frac{I_i}{\sigma} \right)^2$$

where N is the total number of elements within a frame: 10 pixels x 10 pixels x 3 color channels = 300 elements, I is the pixel intensity of each element relative to background in the peak STA frame and σ is the standard deviation of the 300 elements (pixel intensities relative to the background) in the first STA frame. Pixel intensity of each element was divided by this standard deviation to obtain z-scores so that each element had (approximately) a standard normal distribution under the null hypothesis of no signal. We summed the squared z-scores of the peak STA frame and omitted from analysis the 58 cells for which this sum failed to reach a statistical threshold ($p < 0.0001$ χ^2 test, df=300).

We excluded cells that combine cone inputs non-linearly because their STAs do not reflect their stimulus tuning accurately (Horwitz et al., 2005). We identified nonlinear neurons using a non-linearity index (NLI) (Horwitz et al., 2007). The NLI uses the STA and the spike-triggered covariance to find the maximally informative stimulus dimension under a multivariate Gaussian assumption (Pillow, 2006). For each cell, we projected the stimuli shown in the experiment onto the maximally informative dimension and binned the projections, excluding the upper and lower 5% to avoid the influence of outliers. We calculated the average firing rate across the stimuli within each bin. The relationship between firing rate and stimulus projection was fit with three regression equations.

$$y_{linear} = b_0 + b_1 x$$
$$y_{quadratic} = b_0 + b_1 x^2$$

$$y_{full} = b_0 + b_1 x + b_2 x^2$$

The goodness-of-fit of each regression was quantified with an R^2 statistic. The NLI is defined as

$$NLI = \frac{R^2_{quadratic} - R^2_{linear}}{R^2_{full}}$$

The NLI attains its theoretical maximal value of 1 when the inclusion of a linear term does not improve the regression fit. This would be the case, for example, for a V1 complex cell whose response is invariant to contrast polarity. NLI attains its theoretical minimum value of –1 when the inclusion of a quadratic term does not improve the regression fit as would be the case for a purely linear cell. Twenty-four cells were excluded on the basis that their NLI was > 0.

We excluded cells that were spatially non-opponent because these cells cannot be DO or simple. We identified spatially non-opponent cells by analyzing the power spectrum of their spatial weighting functions. Spatially non-opponent cells, by definition, had maximal power in the lowest spatial frequency bin. This criterion excluded 56 cells.

We segregated simple cells from DO cells based on cone weights, and we excluded neurons outside of these categories. Cells were classified as simple if their L- and M-cone weights had the same sign, accounted for 80% of the total cone weight, and individually accounted for at least 10%. Cells were classified as DO if they had large magnitude cone weights of different sign. $DO_{\text{LM-opponent}}$ cells were defined as those that had L- and M-cone weights of opposite sign that together accounted for 80% and individually accounted for at least 30% of the total cone weight. $DO_{\text{S-cone sensitive}}$ cells were cone-opponent and had an S-cone weight that accounted for at least 20% of the total. Forty-one cells that were not categorized as simple, $DO_{\text{LM-opponent}}$, or $DO_{\text{S-cone sensitive}}$ were omitted from the analyses.

Model fitting of the spatial weighting function

We fit the spatial weighting function of each neuron with three models. Fitting was performed using the inbuilt MATLAB *fmincon* function to minimize the sum of squared errors between the spatial weighting function and the model fit. We describe each of the models below.

Gabor model

The Gabor model was defined as:

$$f(x',y') = Ae^{-\frac{\left(x'^2+\gamma^2 y'^2\right)}{2\sigma^2}} cos\left(\left(2\pi y'/\lambda\right)-\phi\right)$$

where (x',y') is obtained by translating the original coordinate frame to the RF center, (x_c,y_c), and rotating it by an angle θ.

$$\begin{aligned} x' &= (x-x_c)\ cos(\theta) + (y-y_c)\ sin(\theta) \\ y' &= -(x-x_c)\ sin(\theta) + (y-y_c)\ cos(\theta) \end{aligned}$$

λ is the spatial period of the cosine component in °/cycle, and ϕ is the spatial phase. A spatial phase of ϕ = 0° gives an even-symmetric RF whereas spatial phase of ϕ = 90° gives an odd-symmetric RF. The two axes of the Gaussian envelope align with the x' and the y' axes. The parameter A is the amplitude, γ is the aspect ratio, and σ is the standard deviation of the Gaussian envelope along the x' axis.

Difference of Gaussians (DoG) model

The Difference of Gaussians (DoG) model can be written:

$$f(x,y) = \frac{A_c}{\sqrt{2\pi\sigma_c^2}} exp(-((x-x_c)^2+(y-y_c)^2)/\sigma_c^2) - \frac{A_s}{\sqrt{2\pi\sigma_s^2}} exp(-((x-x_c)^2+(y-y_c)^2))/\sigma_s^2)$$

where A_c and A_s are the amplitudes of the center and surround. σ_c and σ_s are the standard deviations of the center and surround.

Non-concentric DoG model

$$f(x,y) = \frac{A_c}{\sqrt{2\pi\sigma_c^2}} exp(-((x-x_c)^2+(y-y_c)^2)/\sigma_c^2) - \frac{A_s}{\sqrt{2\pi\sigma_s^2}} exp(-((x-x_s)^2+(y-y_s)^2))/\sigma_s^2)$$

This non-concentric DoG model is identical to the DoG model but has 2 additional parameters (x_s,y_s) that allow the surround to be offset from the center.

Evaluating goodness of model fit

We evaluated the quality of model fits by calculating Pearson's correlation coefficient (R) between the data and the model predictions. To avoid overfitting, we used 5-fold cross validation, fitting the model with 80% of the data and testing the model on the remaining 20%. We report the averaged R across the 5 folds.

Quantifying R as a function of SNR

We used a logistic function to describe R as a function of SNR. The logistic function was defined as:

$$R = \frac{A}{1+e^{-b(SNR-c)}}$$

where A is the maximum value, b is the steepness constant and c is the SNR value at which logistic function is half the maximum value. The fit was determined by maximizing likelihood assuming binomial error.

RESULTS

We analyzed the responses of 207 V1 neurons from 4 macaque monkeys that met our inclusion criteria (**see Methods**). RFs of neurons ranged in eccentricity from 1.7° to 8.42° (median = 4.7°). The number of spikes recorded ranged from 209 to 48106 (median = 2215).

FIGURE 2 HERE

Cone weights

We classified neurons as simple cells or DO cells based on cone weights (**Figure 2**). Simple cells had large magnitude, non-opponent L- and M-cone weights that, together, accounted for 80% of the total cone weight (n=74). DO cells were defined as being cone-opponent and were further classified as LM-opponent (n=95) or S-cone sensitive (n=38) based on cone weight magnitudes and signs. Of the 38 $DO_{\text{S-cone sensitive}}$ neurons recorded, 15 were S-(L+M), 19 were (S+M)-L, and 4 were (S+L)-M.

FIGURE 3 HERE

Model comparison: Gabor vs. DoG

Example STAs from two simple cells and four DO cells are shown (**Figure 3, 1st row**). The cell type classification of each cell can be deduced from its cone weights (**Figure 3, 2nd row**). Simple cell RFs consisted of adjacent ON and OFF regions (**Figure 3A & 3B**). Most simple cell RFs were elongated and clearly oriented (**Figure 3A**), but others were nearly circular and less clearly oriented (**Figure 3B**). RFs of DO cells displayed similar features: some were clearly oriented (**Figures 3C & 3E**) whereas others had nearly circular RF centers and diffuse surrounds (**Figures 3D & 3F**).

To compare the spatial RF organization of simple and DO cells quantitatively, we extracted from each STA the spatial weighting function (**Figure 3, 3rd row**) and fit it with a Gabor model (**Figure 3, 4th row**) and a DoG model (**Figure 3, 5th row**). Goodness-of-fit was quantified with cross-validated R between the data and the model predictions. Elongated RFs were better fit by the Gabor model than the DoG model because the DoG model fit is constrained to be radially symmetric. The example neurons whose RFs were better fit by the DoG model than the Gabor model had a spatial weighting function that was the most nearly radially symmetric by eye (**Figure 3D & 3F**).

FIGURE 4 HERE

The Gabor model outperformed the DoG model for most of the cells tested (141/207, $R_{Gabor} > R_{DoG}$). The superiority of the Gabor model was consistent within each subgroup of cells: simple ($p<0.001$; Wilcoxon signed rank test; **Figure 4A**), $DO_{LM\text{-}opponent}$ ($p=0.02$; **Figure 4B**) and $DO_{S\text{-}cone\ sensitive}$ ($p=0.02$; **Figure 4C**). This result shows that DO cells, like simple cells, have RFs that are more accurately described as Gabor functions than as DoG functions. However, the spatial RFs of simple and DO cells were not identical. The difference between R_{Gabor} and R_{DoG} was larger for simple cells than $DO_{LM\text{-}opponent}$ or $DO_{S\text{-}cone\ sensitive}$ cells ($p<0.001$ for each comparison; simple vs. $DO_{LM\text{-}opponent}$; simple vs. $DO_{S\text{-}cone\ sensitive}$ cells; Mann Whitney U tests). The difference between R_{Gabor} and R_{DoG} was similar for $DO_{LM\text{-}opponent}$ and $DO_{S\text{-}cone\ sensitive}$ cells ($p=0.44$; Mann Whitney U test).

FIGURE 5 HERE

We considered the possibility that the DoG model fit the DO cell data relatively well due to systematic differences in SNR between DO cell STAs and simple cell STAs. For example, a spatial weighting function with low SNR would be fit equally well by a Gabor function as a DoG function even if the true RF organization was a Gabor function. We therefore investigated the relationship between R and the SNR of the peak STA frame for each category of neurons (**see Methods** *for the definition of SNR*). As SNR

increased, so did the goodness-of-fit of the Gabor model, which was similar across the three cell types (p=0.16, Kruskal-Wallis test; **Figure 5A**). This result shows that much of the error in the model fits is due to noise in the STAs and not to systematic errors in the Gabor model fits. Extrapolation with a logistic fit predicts that R_{Gabor} would be 0.85 in the limit of infinite SNR. The Gabor model is therefore not simply a better description than the DoG model; it provides accurate response predictions in absolute terms.

A different result was obtained when SNR was compared to the goodness-of-fit of the DoG model. R_{DoG} was lower for simple cells than for DO cells (**Figure 5B,** median for simple cells 0.38 vs. median for $DO_{\text{LM-opponent}}$ 0.44 vs. median for $DO_{\text{S-cone sensitive}}$ cells 0.43, p=0.09; Kruskal-Wallis test). This difference is clearest for cells with high SNR (p<0.0001, Kruskal-Wallis test on R_{DoG} values for cells with SNRs above the median).

FIGURE 6 HERE

To dissect the differences between simple cell and DO cell RFs more finely, we asked whether simple cell RFs are more frequently odd-symmetric or more elongated than those of DO cells. Either of these properties could degrade the quality of the DoG model fits relative to Gabor fits, because DoG fits are constrained to be even-symmetric and radially symmetric. First, we analyzed the spatial phase of the best-fitting Gabor function, which makes the RF odd-symmetric, even-symmetric, or intermediate (ϕ, **see Methods**). Most simple cells (mean = 57.8°; **Figure 6A**) were odd-symmetric, as were most $DO_{\text{LM-opponent}}$ (mean = 51.2°; **Figure 6B**) and $DO_{\text{S-cone sensitive}}$ cells (mean = 53.1°; **Figure 6C**). The difference in spatial phase did not reach statistical significance, but is in the correct direction to account for the poor DoG model fits to simple cell RFs than DO cell RFs (p=0.21, Kruskal-Wallis test).

Secondly, we analyzed the aspect ratio, which determines how elongated an RF is (γ, **see Methods**). Aspect ratios were larger for simple cells (median = 1.33; **Figure 6D**) than $DO_{\text{LM-opponent}}$ (median = 1.07; **Figure 6E**) and $DO_{\text{S-cone sensitive}}$ cells (median = 0.97; **Figure 6F**). The difference in aspect ratio was statistically significant when all cells were

considered (p=0.04, Kruskal-Wallis test). Restricting our analyses to cells that were better fit by a Gabor model ($R_{Gabor} > R_{DoG}$) agreed qualitatively with the above results (**Figure 6A–F, black histograms**).

FIGURE 7 HERE

The non-concentric DoG model

Gabor and DoG models are classic descriptions of DO RFs, but recently a third model was proposed: the center, crescent-shaped surround model (Conway, 2001; Conway & Livingstone, 2006). We formalized this idea by modifying the DoG model to allow the center and surround Gaussians to be non-concentric (**see Methods**). This model captures many of the diverse RF structures we observed in our data (**Figure 7A**).

We compared the quality of Gabor and non-concentric DoG fits for each cell. Simple cell RFs were better fit by the Gabor model ($p<0.001$; Wilcoxon signed rank test; **Figure 7B**) but $DO_{LM\text{-opponent}}$ cells and $DO_{S\text{-cone sensitive}}$ cell RFs were fit similarly by both the models ($p > 0.2$; Wilcoxon signed rank tests; **Figure 7B and 7D**). These results suggest that the non-concentric DoG model performed similarly to the Gabor model for DO cell RFs but poorly for simple cell RFs. Note that the non-concentric DoG model is purely descriptive; that the cone-opponent mechanisms that underlie the RFs of DO cells may not overlap spatially.

DISCUSSION

We analyzed the spatial RFs of macaque V1 DO and simple cells with white noise RF mapping, model fitting, and statistical comparisons. To the best of our knowledge, this is the first study to compare DO and simple cell RFs using the same stimulus set. We report three new results. First, the RFs of DO and simple cells were more accurately described by a Gabor model than a DoG model. Second, DO cells tend to have odd-symmetric RFs, similarly to simple cells. Third, we formalized a previously proposed qualitative model and found that it performed similarly to the Gabor model for DO cells but poorly for simple cells. Together, our results show that most DO cells lack a center-surround RF organization, the spatial RFs of simple and DO cells are broadly similar, and a center-crescent surround model describes DO cell RFs nearly as accurately as a Gabor model.

Below, we compare our results to those of previous studies. We then discuss the robustness of our results to the criteria used to categorize cells and the use of R as a measure of goodness-of-fit. Finally, we discuss the potential roles of DO cells in image processing and how our findings have constrained these roles.

Comparison with previous work

Different studies have reached different conclusions about the spatial structure of DO RFs in monkey V1 (Conway, 2001; Conway & Livingstone, 2006; Hubel & Wiesel, 1968; Johnson et al., 2001, 2004, 2008; M. S. Livingstone & Hubel, 1984; Michael, 1978; Poggio, 1975). Early investigations, mostly using circular spots of light were entirely qualitative and reported DO cells to have a concentric center-surround RF organization (Hubel & Wiesel, 1968; M. S. Livingstone & Hubel, 1984; Michael, 1978; Poggio, 1975). Later investigations using sparse noise stimuli measured 2-D RF structure and proposed that DO cell RFs have circular centers and crescent-shaped surrounds (Conway, 2001; Conway & Livingstone, 2006). Parallel investigations using drifting and rapidly flashed sinusoidal gratings concluded that DO cells have Gabor-like RFs largely

on the basis of 1-dimensional measurements (orientation-tuning curves) (Johnson et al., 2001, 2004, 2008).

The lack of consensus about DO cell RF structure may reflect biases produced by different stimulus sets and incomplete RF descriptions. Sparse noise stimuli have the advantage of stimulating different parts of the RF independently and thus make no assumptions about the spatial structure of the RF (Conway, 2001; Conway & Livingstone, 2006). However, spiking nonlinearities can prevent simultaneous cone-isolating increments and decrements from cancelling, even outside of the RF, potentially producing an appearance of spatial opponency where none exists (Ben Lankow and Mark Goldman, personal communication).

Sinusoidal gratings are powerful tools for identifying the RF structure of neurons that are well described by a linear model (DeAngelis, 1993; Movshon, Thompson, & Tolhurst, 1978; Shapley, 2009). However, many V1 neurons are nonlinear, for example, complex cells. Some studies included complex cells in the population of DO cells (Johnson et al., 2001, 2004, 2008). Complex cells are poorly described by a linear model and do not abide by the definition of double-opponency because they do not have opposite color preferences in different parts of their RFs (Daw, 1968; M. S. Livingstone & Hubel, 1984).

We examined the RFs of simple cells and DO cells with the same stimuli and data analysis. We used a stimulus that provides accurate STA measurements irrespective of spiking nonlinearities and we excluded complex cells for our analyses (Chichilnisky, 2001). We found that simple cell RFs are better fit by the Gabor model than the DoG model or non-concentric DoG model, consistent with previous studies (D. L. Ringach, Shapley, R. M., & Hawken, M. J., 2002). Most simple cells had odd symmetric RFs, a result that is also consistent with a previous report (D. L. Ringach, 2002). A novel contribution of the current study is the extension of this result to DO cells.

Effects of cell categorization criteria

We distinguished simple cells from DO cells based on cone weights. We applied a stricter criterion to L- and M-cone weights to categorize a cell as simple than as $DO_{LM\text{-}opponent}$—a fact that is visible from the greater spread of L- and M-cone weights for simple cells than $DO_{LM\text{-}opponent}$ cells (**Figure 2**). The rationale for this decision is the greater variability in estimated cone weights for non-opponent cells (Horwitz et al., 2007). Nevertheless, our results are robust to this decision. We recategorized the cells into $DO_{LM\text{-}opponent}$ and simple categories with reversed criteria (**see Methods** for the original criteria) and obtained similar results to those shown in the main text (**Figure S1–2**).

Effects of using R as a measure for model comparison

We compared the quality of model fits using cross-validated R between data and model predictions, but our results are robust to this choice. We repeated the model comparisons using the Bayesian Information Criterion, cross validated mean squared error and cross validated probability of predicted spikes in response to white noise stimuli. The results from all of these analyses agreed qualitatively with those reported in the main text (**Figure S3–4**).

Role of DO cells in image processing

DO cells carry information about the phase and orientation of local chromatic variations. This information may be useful for at least two visual computations. First, DO cells might aid in shape-from-shading. Extraction of chromatic orientation flows in 2-D images is critical for accurate perception of 3-D shapes (Kingdom, 2003; Kunsberg, 2018; Zaidi, 2006). In some displays, alignment of chromatic and luminance edges suppresses the percept of 3-D form whereas misalignment enhances the 3-D percept (Kingdom, 2003). Signals from DO cells may therefore be integrated with those from simple cells to infer 3-D structure from 2-D retinal images. Second, DO cells might aid in inferring whether an edge in a visual scene is caused by the same material under different lighting conditions or by two different materials under the same lighting condition. An edge

between two pieces of a single material under direct illumination and in shadow creates a nearly pure intensity difference. On the contrary, an edge between two different materials under the same illumination creates spatially coincident intensity and spectral variations. The presence or absence of a spectral variation could serve as an important cue to the visual system for disambiguating material edges from illumination edges (Cavanagh, 1991; Fine, 2003; Olmos, 2004; Tappen, 2003). The similarity of RF structure between simple cells and DO cells might facilitate downstream integration of their responses.

FIGURE 8 HERE

Are DO cells cone-opponent simple cells?

The similarity of spatial RF structure between DO and simple cells motivates the hypothesis that the primary difference between these two cell types is the sign of input they receive (indirectly) from the three cone classes. Indeed, the models proposed to underlie simple cell RFs can also be applied to DO cells with only a minor change in the wiring (**Figure 8**).

A hallmark of simple cells is spatial linearity, a property mediated in part by push-pull excitation and inhibition (D. Ferster, 1988; D. Ferster, & Miller, K. D., 2000; Hirsch, 1998; Tolhurst, 1990). Some DO cells exhibit push-pull responses, consistent with the proposed similarly between them and simple cells (Conway 2006). However, whether the departures from linearity observed in some DO cells exceeds expectations provided by the benchmark of simple cells is unclear. To answer this question, a useful next step would be to compare quantitatively the degree of spatial linearity between DO and simple cells.

ACKNOWLEDGEMENTS

We thank Fred Rieke, Adrienne L. Fairhall, Scott O. Murray and John C. Tuthill for helpful discussions on the earlier stage of the work. This work was funded by NIH EY018849 to Gregory D. Horwitz, NIH/ORIP grant P51OD010425, and NEI Center Core Grant for Vision Research P30 EY01730 to the University of Washington and R90 DA033461 (Training Program in Neural Computation and Engineering) to Abhishek De.

FIGURE LEGENDS

Figure 1. Derivation of cone weights and spatial weighting function **A.** Computing the weighted STA (the weighted sum of the peak STA frame and two flanking frames)(right) from spike triggered white noise stimuli (left). **B.** Singular value decomposition (SVD) of the weighted STA reveals cone weights and spatial weighting function. **C.** Reconstructing a low-rank approximation of the weighted STA by multiplying cone weights and spatial weighting function. Subtracting the weighted STA from the the low-rank approximation yields the residual, which has little structure. **D.** Percent explained variance plotted against the three sets of singular vectors for the example cell and the population (mean ± SD). Cone weights and the spatial weighting function constitute the 1^{st} singular vectors. Percent explained variance was derived from the singular values using SVD over entire 10 pixels x 10 pixels of spatial weighting function (filled black circles) and omitting pixels outside of the RF (filled black squares).

Figure 2. Normalized cone weights of simple (black), $DO_{\text{LM-opponent}}$ (red), $DO_{\text{S-cone sensitive}}$ (blue) and unclassified (gray) cells. M-cone weights were constrained to be positive. Points closer to the origin have larger S-cone weights than those far from the origin.

Figure 3. Gabor and Difference of Gaussians (DoG) model fits to spatial weighting functions of six example cells. The quality of each model fit was quantified using cross-validated *R*. **A.** a simple cell with R_{Gabor}= 0.77 and R_{DoG}= 0.45 **B.** a simple cell with R_{Gabor}= 0.67 and R_{DoG}= 0.59 **C.** a $DO_{\text{LM-opponent}}$ with R_{Gabor}= 0.45 and R_{DoG}= 0.30 **D.** a $DO_{\text{LM-opponent}}$ cell with R_{Gabor}= 0.90 and R_{DoG}= 0.91 **E.** a $DO_{\text{S-cone sensitive}}$ cell with R_{Gabor}= 0.69 and R_{DoG}= 0.63 **F.** a $DO_{\text{S-cone sensitive}}$ cell with R_{Gabor}= 0.46 and R_{DoG}= 0.49.

Figure 4. Comparison of Gabor and DoG model fits. Cross-validated R from Gabor fits is plotted against DoG fits for simple (**A**), $DO_{\text{LM-opponent}}$ (**B**), and $DO_{\text{S-cone sensitive}}$ cells (**C**). Five example STAs are shown in each panel to illustrate the diversity of RF structures observed and their relationship to R.

Figure 5. Analyses of Gabor and DoG model fits **A.** Scatterplot of cross-validated R of Gabor fits vs. signal-to-noise ratios (SNR) of peak STA frames for simple cells (black), $DO_{\text{LM-opponent}}$ cells (red) and $DO_{\text{S-cone sensitive}}$ cells (blue). **B.** Identical to **A** but plotted for DoG fits.

Figure 6. Analyses of Gabor model parameters for all cells (white) and cells that are better fit by the Gabor model than the DoG model (black). **A.** Best fitting phase (ϕ) of Gabor fits to simple cell spatial weighting functions. The mean ϕ is 57.8° for all simple RFs and 58.1° for cells better fit by Gabor model. **B & C** Identical to **A** but for $DO_{\text{LM-opponent}}$ cells and $DO_{\text{S-cone sensitive}}$ cells, respectively. The mean ϕ is 51.2° for all $DO_{\text{LM-opponent}}$ RFs and 54.5° for cells better fit by Gabor model. The mean ϕ is 53.1° for all $DO_{\text{S-cone sensitive}}$ RFs and 50.7° for cells better fit by Gabor model. **D.** Best fitting aspect ratio (γ) of Gabor fits to simple cell spatial weighting functions. The median γ was 1.33 for all simple cell RFs and those that were better fit by Gabor model. **E & F.** Identical to **D** but for $DO_{\text{LM-opponent}}$ cells and $DO_{\text{S-cone sensitive}}$ cells, respectively, The median γ was 1.07 for all $DO_{\text{LM-opponent}}$ RFs and 1.15 for cells better fit by Gabor model. **F.** The median γ was 0.97 for all $DO_{\text{S-cone sensitive}}$ RFs and 1.00 for cells better fit by Gabor model than DoG model.

Figure 7. Comparison of non-concentric DoG and Gabor model fits **A.** Non-concentric DoG fits to data of the six example cells from **Fig 3.** $R_{non-concentric\ \ DoG}$= 0.54, 0.66, 0.41, 0.90, 0.68 and 0.47 from left to right. R from Gabor fits are plotted against R from non-concentric DoG fits for simple (**B**), $DO_{\text{LM-opponent}}$ cells (**C**), and $DO_{\text{S-cone sensitive}}$ cells (**D**).

Figure 8. Schematic diagram of the circuitry proposed to underlie simple cell and DO RFs. **A.** A simple cell RF constructed from parvocellular LGN afferents. The ON subregion (L+M) is excited by L-ON and M-ON LGN cells and is inhibited by L-OFF and M-OFF LGN cells. Similarly, the OFF subregion (-L-M) is excited by L-OFF and M-OFF LGN cells and is inhibited by L-ON and M-ON LGN cells. **B.** Construction of a DO cell

RF using the same set of parvocellular LGN cells that provide input to a simple cell. The L-M subregion is excited by L-ON and M-OFF LGN cells and is inhibited by L-OFF and M-ON LGN cells whereas the M-L subregion is excited by L-OFF and M-ON LGN cells and is inhibited by L-ON and M-OFF LGN cells.

SUPPLEMENTAL FIGURE LEGENDS

Figure S1. Reclassification of cells with reversed cone weight criteria. Shown are the normalized cone weights of simple (black), $DO_{LM\text{-}opponent}$ (red), $DO_{S\text{-}cone\ sensitive}$ (blue) and unclassified (gray) cells. M-cone weights were constrained to be positive. Cells were classified as simple if the L- and M-cone weights had the same sign, that together, accounted for 80% of the total cone weight and individually accounted for at least 30%. Cells were labeled as $DO_{LM\text{-}opponent}$ if the L- and M-cone weights had opposite sign, together accounted for 80% and individually accounted for at least 10% of the total cone weight. Classification of $DO_{S\text{-}cone\ sensitive}$ was same as the original as described in the Methods. The remaining cells were labeled as unclassified.

Figure S2. Model comparisons after reclassification of cells. **A.** Cross-validated R from Gabor fit is plotted against DoG fit for simple cells. **B.** Identical to **A** but for $DO_{LM\text{-}opponent}$ cells. **C.** Analyses of best fitting phase (ϕ) of Gabor fits to all simple RFs (white) and those that are better fit by the Gabor model than the DoG model (black). The mean ϕ is 60.6° for simple RFs and 61.8° for cells better fit by Gabor model. **D.** Identical to **C** but for $DO_{LM\text{-}opponent}$ RFs. The mean ϕ is 55.0° for all $DO_{LM\text{-}opponent}$ RFs and 59.4° for cells better fit by Gabor model. **E.** Analyses of best fitting aspect ratio (γ) of Gabor fits to all simple RFs (white) and those that are better fit by the Gabor model than the DoG model (black). The median γ is 1.30 for all simple cell RFs and 1.34 for cells better fit by Gabor model. **F.** Identical to **E** but for $DO_{LM\text{-}opponent}$ RFs. The median γ is 1.09 for all simple cell RFs and 1.18 for cells better fit by Gabor model. **G.** Cross-validated R from Gabor fit is plotted against non-concentric DoG fit for simple cells. **H.** Identical to **G** but for $DO_{LM\text{-}opponent}$ cells.

Figure S3. Comparison of Gabor and DoG model fits. Plotted are the results from three different analyses to compare model fits to the spatial RFs of simple, $DO_{LM\text{-}opponent}$ and $DO_{S\text{-}cone\ sensitive}$ cells. **A.** Cross-validated spike predictability using receiver operating characteristics (ROC) from Gabor fits is plotted against the DoG fits for simple cells. **B.** Identical to **A.** but for $DO_{LM\text{-}opponent}$ cells. **C.** Identical to **A.** but for $DO_{S\text{-}cone\ sensitive}$ cells. **D.**

Cross-validated sum of squared errors (SSE) from Gabor fits is plotted against the DoG fits for simple cells. **E.** Identical to **D.** but for $DO_{LM\text{-}opponent}$ cells. **F.** Identical to **D.** but for $DO_{S\text{-}cone\ sensitive}$ cells. **G.** Bayesian Information Criteria (BIC) from Gabor fits is plotted against the DoG fits for simple cells. A better model fit yields a lower BIC. **H.** Identical to **G.** but for $DO_{LM\text{-}opponent}$ cells. **I.** Identical to **G.** but for $DO_{S\text{-}cone\ sensitive}$ cells.

Figure S4. Comparison of Gabor and non-concentric DoG model fits. Plotted are the results from three different analyses to compare model fits to the spatial RFs of simple, $DO_{LM\text{-}opponent}$ and $DO_{S\text{-}cone\ sensitive}$ cells. **A.** Cross-validated spike predictability using receiver operating characteristics (ROC) from Gabor fits is plotted against the non-concentric DoG fits for simple cells. **B.** Identical to **A.** but for $DO_{LM\text{-}opponent}$ cells. **C.** Identical to **A.** but for $DO_{S\text{-}cone\ sensitive}$ cells. **D.** Cross-validated sum of squared errors (SSE) from Gabor fits is plotted against the non-concentric DoG fits for simple cells. **E.** Identical to **D.** but for $DO_{LM\text{-}opponent}$ cells. **F.** Identical to **D.** but for $DO_{S\text{-}cone\ sensitive}$ cells. **G.** Bayesian Information Criteria (BIC) from Gabor fits is plotted against the non-concentric DoG fits for simple cells. A better model fit yields a lower BIC. **H.** Identical to **G.** but for $DO_{LM\text{-}opponent}$ cells. **I.** Identical to **G.** but for $DO_{S\text{-}cone\ sensitive}$ cells.

REFERENCES

1. Brainard, D. H. (1997). The Psychophysics Toolbox. *Spat Vis, 10*(4), 433-436.
2. Cavanagh, P. (1991). Vision at equiluminance. Vision and visual dysfunction: Limits of vision, 5, 234-250.
3. Chichilnisky, E. J. (2001). A simple white noise analysis of neuronal light responses. *Network, 12*(2), 199-213.
4. Conway, B. R. (2001). Spatial structure of cone inputs to color cells in alert macaque primary visual cortex (V-1). *Journal of Neuroscience, 21*(8), 2768-2783.
5. Conway, B. R., & Livingstone, M. S. (2006). Spatial and temporal properties of cone signals in alert macaque primary visual cortex. *J Neurosci, 26*(42), 10826-10846.
6. Daw, N. W. (1968). Colour-coded ganglion cells in the goldfish retina: extension of their receptive fields by means of new stimuli. *The Journal of physiology, 197*(3), 567-592.
7. DeAngelis, G. C., Ohzawa, I., & Freeman, R. D. (1993). Spatiotemporal organization of simple-cell receptive fields in the cat's striate cortex. II. Linearity of temporal and spatial summation. *Journal of Neurophysiology, 69*(4), 1118-1135.
8. Derrington, A. M., Krauskopf, J., & Lennie, P. (1984). Chromatic mechanisms in lateral geniculate nucleus of macaque. *J Physiol, 357*, 241-265.
9. Ferster, D. (1988). Spatially opponent excitation and inhibition in simple cells of the cat visual cortex. *Journal of Neuroscience, 8*(4), 1172-1180.
10. Ferster, D., & Miller, K. D. (2000). Neural mechanisms of orientation selectivity in the visual cortex. *Annual review of neuroscience, 23*(1), 441-471.
11. Fine, I., MacLeod, D. I., & Boynton, G. M. (2003). Surface segmentation based on the luminance and color statistics of natural scenes. *JOSA A, 20*(7), 1283-1291.
12. Gregory, R. L. (1977). Vision with isoluminant colour contrast: 1. A projection technique and observations. *Perception, 6*(1), 113-119.
13. Hirsch, J. A., Alonso, J. M., Reid, R. C., & Martinez, L. M. (1998). Synaptic integration in striate cortical simple cells. *Journal of neuroscience, 18*(22), 9517-9528.

14. Horwitz, G. D., & Albright, T. D. (2005). Paucity of chromatic linear motion detectors in macaque V1. *J Vis, 5*(6), 525-533.
15. Horwitz, G. D., Chichilnisky, E. J., & Albright, T. D. (2005). Blue-yellow signals are enhanced by spatiotemporal luminance contrast in macaque V1. *Journal of Neurophysiology, 93*(4), 2263-2278.
16. Horwitz, G. D., Chichilnisky, E. J., & Albright, T. D. (2007). Cone inputs to simple and complex cells in V1 of awake macaque. *Journal of Neurophysiology, 97*(4), 3070-3081.
17. Hubel, D. H., & Wiesel, T. N. (1968). Receptive fields and functional architecture of monkey striate cortex. *J Physiol, 195*(1), 215-243.
18. Johnson, E. N., Hawken, M. J., & Shapley, R. (2001). The spatial transformation of color in the primary visual cortex of the macaque monkey. *Nat Neurosci, 4*(4), 409-416.
19. Johnson, E. N., Hawken, M. J., & Shapley, R. (2004). Cone inputs in macaque primary visual cortex. *Journal of Neurophysiology, 91*(6), 2501-2514.
20. Johnson, E. N., Hawken, M. J., & Shapley, R. (2008). The orientation selectivity of color-responsive neurons in macaque V1. *J Neurosci, 28*(32), 8096-8106.
21. Jones, J. P., & Palmer, L. A. (1987). An evaluation of the two-dimensional Gabor filter model of simple receptive fields in cat striate cortex. *Journal of neurophysiology, 58*(6), 1233-1258.
22. Kingdom, F. A. (2003). Color brings relief to human vision. *Nature neuroscience, 6*(6).
23. Kunsberg, B., Holtmann-Rice, D., Alexander, E., Cholewiak, S., Fleming, R., & Zucker, S. W. (2018). Colour, contours, shading and shape: flow interactions reveal anchor neighbourhoods. *Interface focus, 8*(4).
24. Lennie, P., Krauskopf, J., & Sclar, G. (1990). Chromatic mechanisms in striate cortex of macaque. *J Neurosci, 10*(2), 649-669.
25. Livingstone, M. S., & Hubel, D. H. (1987). Psychophysical evidence for separate channels for the perception of form, color, movement, and depth. *Journal of Neuroscience, 7*(11), 3416-3468.

26. Livingstone, M. S., & Hubel, D. H. (1984). Anatomy and physiology of a color system in the primate visual cortex. *J Neurosci, 4*(1), 309-356.
27. McIlhagga, W., & Mullen, K. T. (2018). Evidence for chromatic edge detectors in human vision using classification images. *Journal of vision, 18*(9).
28. Michael, C. R. (1978). Color vision mechanisms in monkey striate cortex: dual-opponent cells with concentric receptive fields. *Journal of Neurophysiology, 41*(3), 572-588.
29. Moore IV, B. D., & Freeman, R. D. (2012). Development of orientation tuning in simple cells of primary visual cortex. *Journal of neurophysiology, 107*(9), 2506-2516.
30. Movshon, J. A., Thompson, I. D., & Tolhurst, D. J. (1978). Spatial summation in the receptive fields of simple cells in the cat's striate cortex. *J Physiol, 283*, 53-77.
31. Mullen, K. T., & Beaudot, W. H. (2002). Comparison of color and luminance vision on a global shape discrimination task. *Vision Research, 42*(5), 565-575.
32. Olmos, A., & Kingdom, F. A. (2004). A biologically inspired algorithm for the recovery of shading and reflectance images. *Perception, 33*(12), 1463-1473.
33. Pillow, J. W., & Simoncelli, E. P. (2006). Dimensionality reduction in neural models: an information-theoretic generalization of spike-triggered average and covariance analysis. *Journal of vision, 6*(4).
34. Poggio, G. F., Baker, F. H., Mansfield, R. J. W., Sillito, A., & Grigg, P. (1975). Spatial and chromatic properties of neurons subserving foveal and parafoveal vision in rhesus monkey. *Brain research, 100*(1), 25-59.
35. Ringach, D. L. (2002). Spatial structure and symmetry of simple-cell receptive fields in macaque primary visual cortex. *Journal of neurophysiology, 88*(1), 455-463.
36. Ringach, D. L., Shapley, R. M., & Hawken, M. J. (2002). Orientation selectivity in macaque V1: diversity and laminar dependence. *Journal of Neuroscience, 22*(13), 5639-5651.
37. Rodieck, R. W. (1965). Quantitative analysis of cat retinal ganglion cell response to visual stimuli. *Vision research, 5*(12), 583-601.
38. Shapley, R. (2009). Linear and nonlinear systems analysis of the visual system: Why does it seem so linear?: A review dedicated to the memory of Henk Spekreijse. *Vision research, 49*(9), 907-921.

39. Spitzer, H., & Barkan, Y. (2005). Computational adaptation model and its predictions for color induction of first and second orders. *Vision Research, 45*(27), 3323-3342.
40. Tappen, M. F., Freeman, W. T., & Adelson, E. H. (2003). Recovering intrinsic images from a single image. *In Advances in neural information processing systems*, 1367-1374.
41. Tolhurst, D. J., & Dean, A. F. (1990). The effects of contrast on the linearity of spatial summation of simple cells in the cat's striate cortex. *Experimental Brain Research, 79*(3), 582-588.
42. Weller, J. P., & Horwitz, G. D. (2018). Measurements of neuronal color tuning: Procedures, pitfalls, and alternatives. *Vision Research, 151*, 53-60.
43. Zaidi, Q., & Li, A. (2006). Three-dimensional shape perception from chromatic orientation flows. *Visual Neuroscience, 23*(3-4), 323-330.

Figure 1

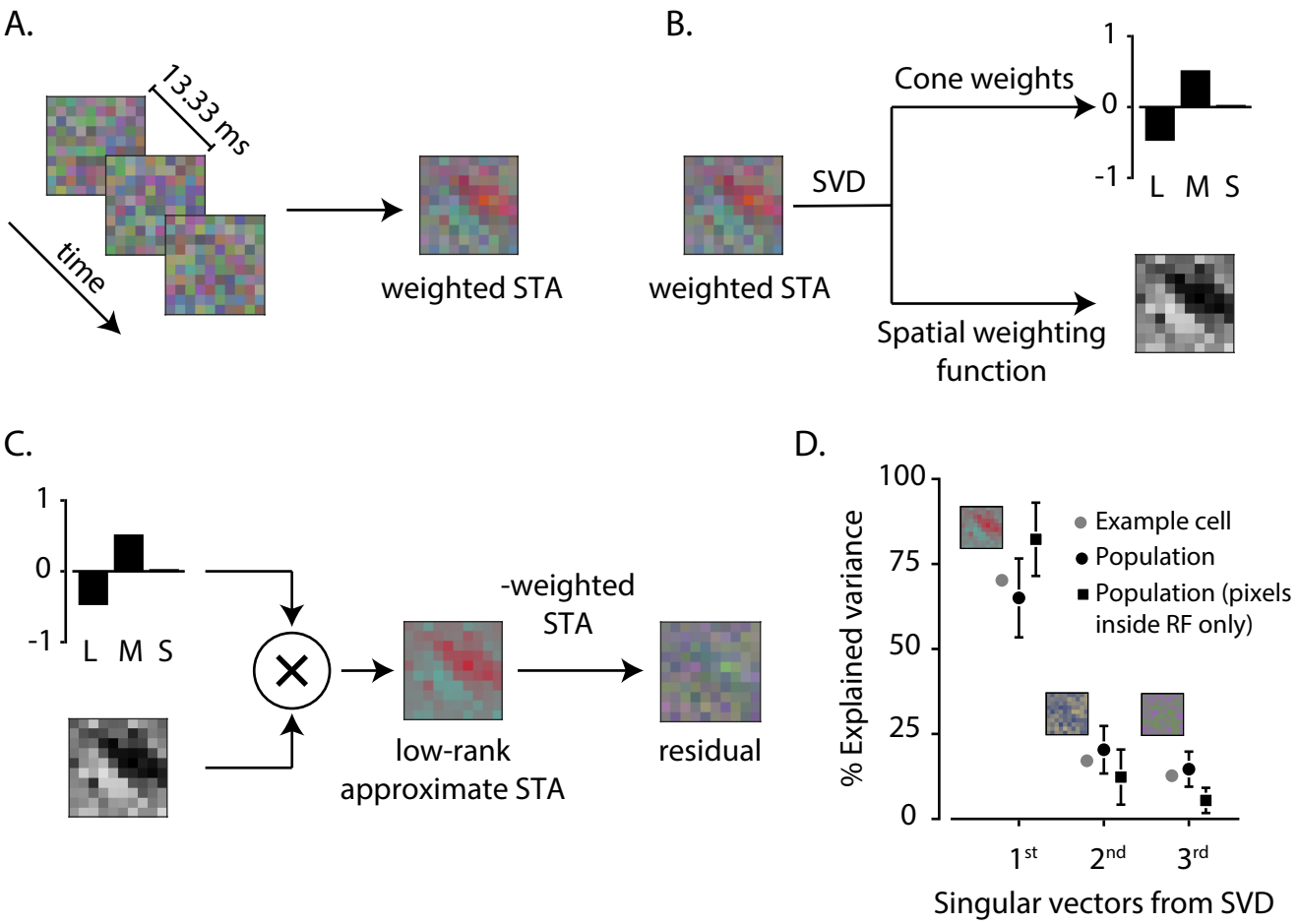

Figure 1. Derivation of cone weights and spatial weighting function **A.** Computing the weighted STA (the weighted sum of the peak STA frame and two flanking frames)(right) from spike triggered white noise stimuli (left). **B.** Singular value decomposition (SVD) of the weighted STA reveals cone weights and spatial weighting function. **C.** Reconstructing a low-rank approximation of the weighted STA by multiplying cone weights and spatial weighting function. Subtracting the weighted STA from the the low-rank approximation yields the residual, which has little structure. **D.** Percent explained variance plotted against the three sets of singular vectors for the example cell and the population (mean ± SD). Cone weights and the spatial weighting function constitute the 1st singular vectors. Percent explained variance was derived from the singular values using SVD over entire 10 pixels x 10 pixels of spatial weighting function (filled black circles) and omitting pixels outside of the RF (filled black squares).

Figure 2

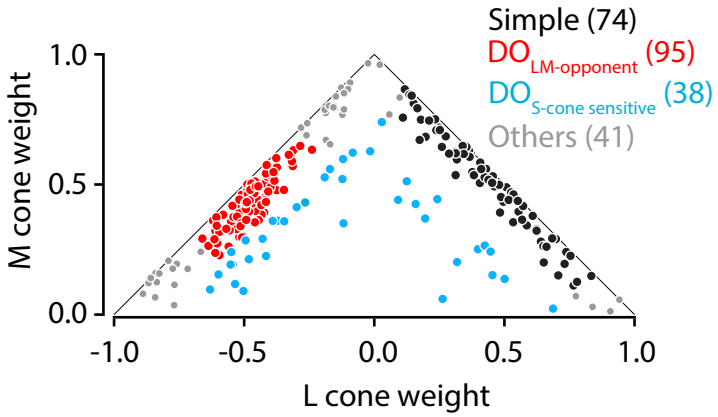

Figure 2. Normalized cone weights of simple (black), $DO_{LM\text{-}opponent}$ (red), $DO_{S\text{-}cone\ sensitive}$ (blue) and unclassified (gray) cells. M-cone weights were constrained to be positive. Points closer to the origin have larger S-cone weights than those far from the origin.

Figure 3

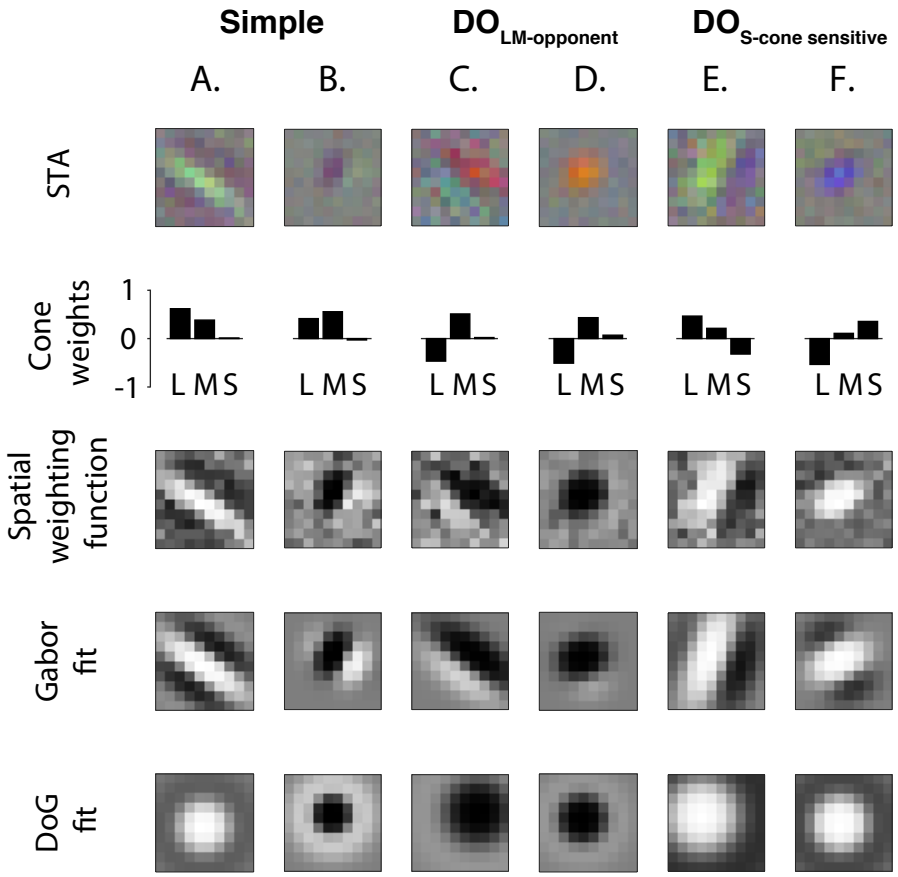

Figure 3. Gabor and Difference of Gaussians (DoG) model fits to spatial weighting functions of six example cells. The quality of each model fit was quantified using cross-validated R. **A.** a simple cell with R_{Gabor}= 0.77 and R_{DoG}= 0.45 **B.** a simple cell with R_{Gabor}= 0.67 and R_{DoG}= 0.59 **C.** a $DO_{LM\text{-}opponent}$ with R_{Gabor}= 0.45 and R_{DoG}= 0.30 **D.** a $DO_{LM\text{-}opponent}$ cell with R_{Gabor}= 0.90 and R_{DoG}= 0.91 **E.** a $DO_{S\text{-}cone\ sensitive}$ cell with R_{Gabor}= 0.69 and R_{DoG}= 0.63 **F.** a $DO_{S\text{-}cone\ sensitive}$ cell with R_{Gabor}= 0.46 and R_{DoG}= 0.49.

Figure 4

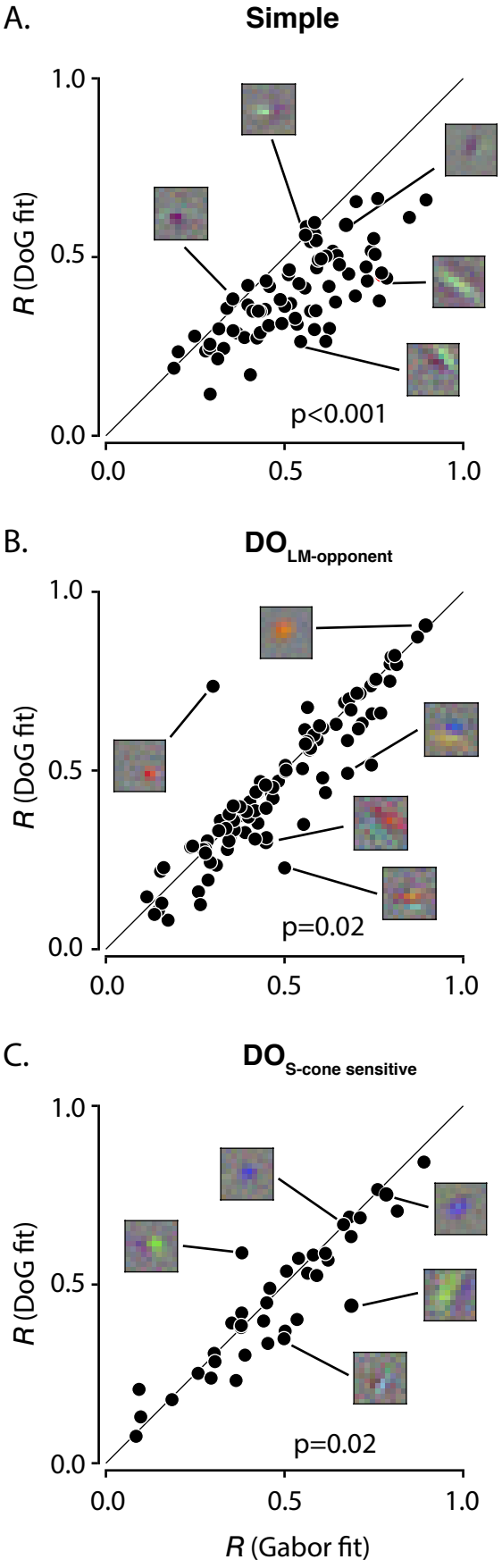

Figure 4. Comparison of Gabor and DoG model fits. Cross-validated *R* from Gabors fit is plotted against DoG fits for simple (**A**), $DO_{LM\text{-}opponent}$ (**B**), and $DO_{S\text{-}cone\ sensitive}$ cells (**C**). Five example STAs are shown in each panel to illustrate the diversity of RF structures observed and their relationship to *R*.

Figure 5

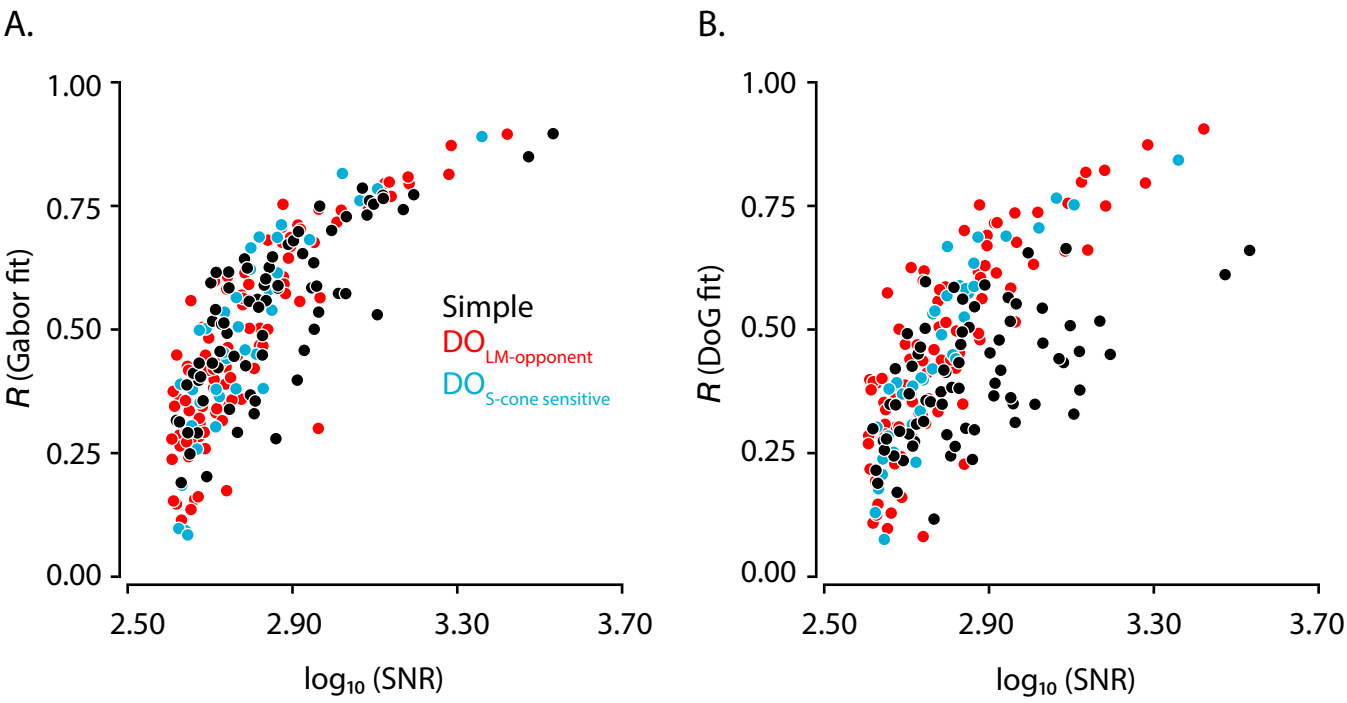

Figure 5. Analyses of Gabor and DoG model fits **A.** Scatterplot of cross-validated *R* of Gabor fits vs. signal-to-noise ratios (SNR) of peak STA frames for simple cells (black), $DO_{LM\text{-}opponent}$ cells (red) and $DO_{S\text{-}cone\ sensitive}$ cells (blue). **B.** Identical to **A** but plotted for DoG fits.

Figure 6

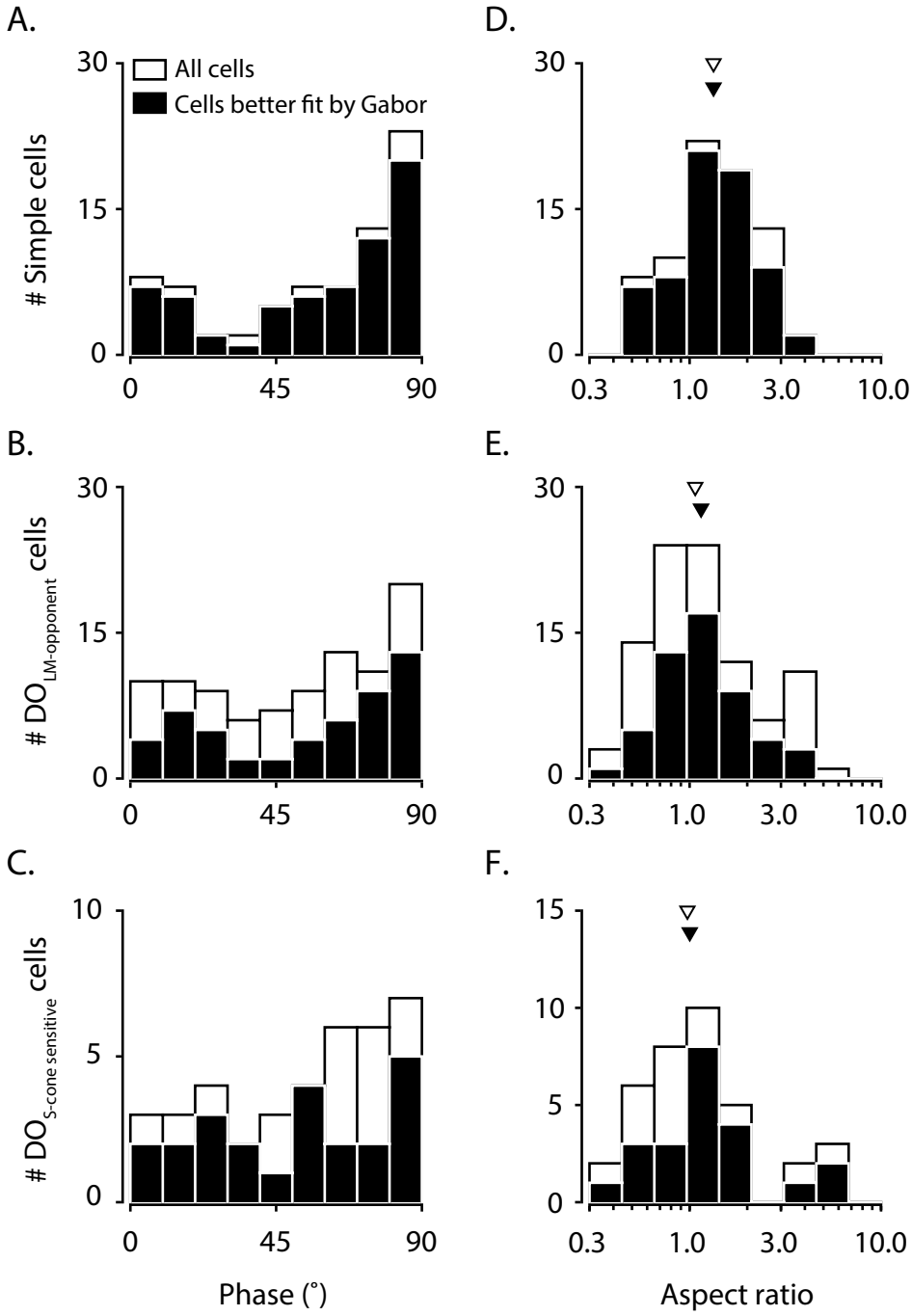

Figure 6. Analyses of Gabor model parameters for all cells (white) and cells that are better fit by the Gabor model than the DoG model (black). **A.** Best fitting phase (φ) of Gabor fits to simple cell spatial weighting functions. The mean φ is 57.8° for all simple RFs and 58.1° for cells better fit by Gabor model. **B & C.** Identical to **A** but for $DO_{LM\text{-}opponent}$ cells and $DO_{S\text{-}cone\ sensitive}$ cells, respectively. The mean φ is 51.2° for all $DO_{LM\text{-}opponent}$ RFs and 54.5° for cells better fit by Gabor model. The mean φ is 53.1° for all $DO_{S\text{-}cone\ sensitive}$ RFs and 50.7° for cells better fit by Gabor model. **D.** Best fitting aspect ratio (γ) of Gabor fits to simple cell spatial weighting functions. The median γ was 1.33 for all simple cell RFs and those that were better fit by Gabor model. **E & F.** Identical to D but for $DO_{LM\text{-}opponent}$ cells and $DO_{S\text{-}cone\ sensitive}$ cells, respectively, The median γ was 1.07 for all $DO_{LM\text{-}opponent}$ RFs and 1.15 for cells better fit by Gabor model. The median γ was 0.97 for all $DO_{S\text{-}cone\ sensitive}$ RFs and 1.00 for cells better fit by Gabor model than DoG model.

Figure 7

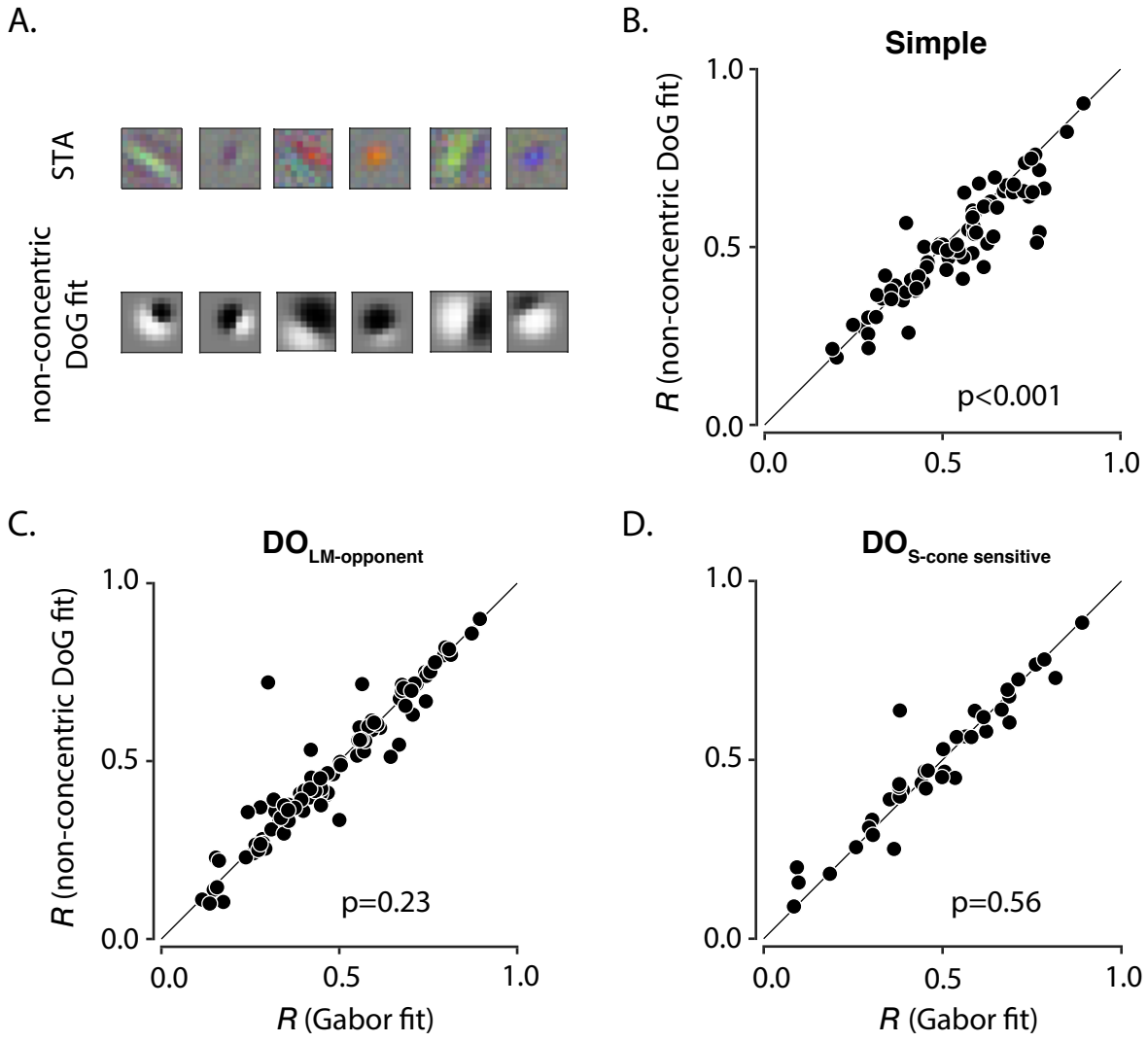

Figure 7. Comparison of non-concentric DoG and Gabor model fits **A.** Non-concentric DoG fits to data of the six example cells from **Fig 3.** $R_{\text{non-concentric DoG}}$ = 0.54, 0.66, 0.41, 0.90, 0.68 and 0.47 from left to right. *R* from Gabor fits are plotted against *R* from non-concentric DoG fits for simple (**B**), $DO_{\text{LM-opponent}}$ cells (**C**), and $DO_{\text{S-cone sensitive}}$ cells (**D**).

Figure 8

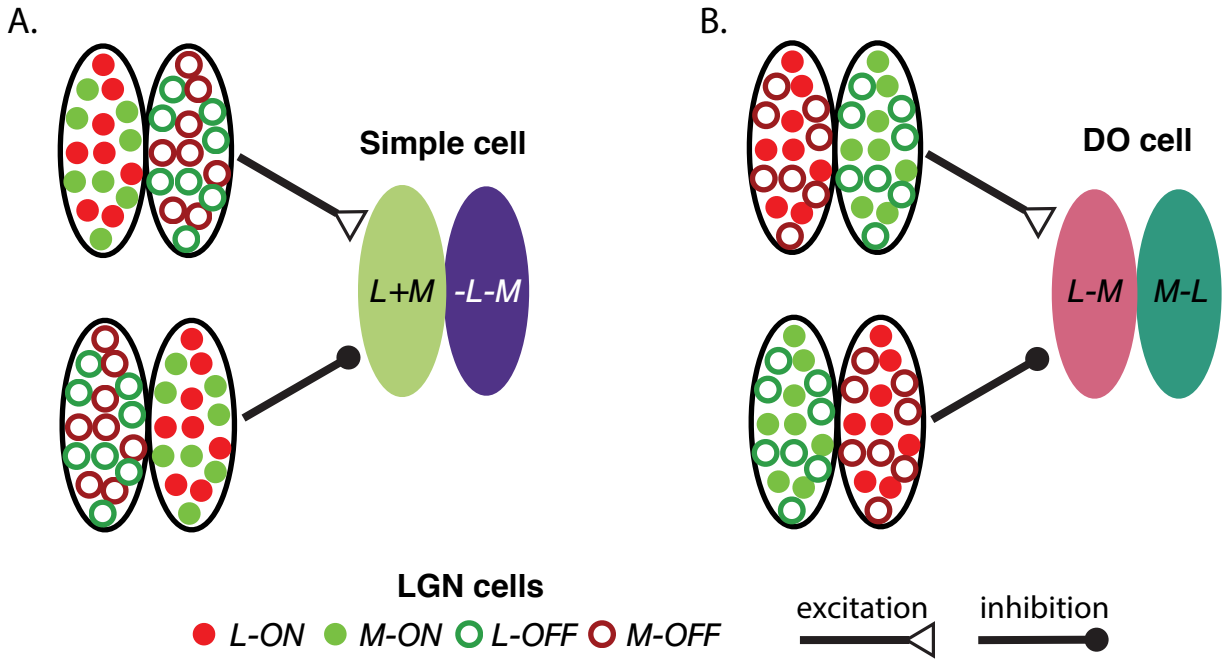

Figure 8. Schematic diagram of the circuitry proposed to underlie simple cell and DO RFs. **A.** A simple cell RF constructed from parvocellular LGN afferents. The ON subregion (L+M) is excited by L-ON and M-ON LGN cells and is inhibited by L-OFF and M-OFF LGN cells. Similarly, the OFF subregion (-L-M) is excited by L-OFF and M-OFF LGN cells and is inhibited by L-ON and M-ON LGN cells. **B.** Construction of a DO cell RF using the same set of parvocellular LGN cells that provide input to a simple cell. The L-M subregion is excited by L-ON and M-OFF LGN cells and is inhibited by L-OFF and M-ON LGN cells whereas the M-L subregion is excited by L-OFF and M-ON LGN cells and is inhibited by L-ON and M-OFF LGN cells.

Figure S1

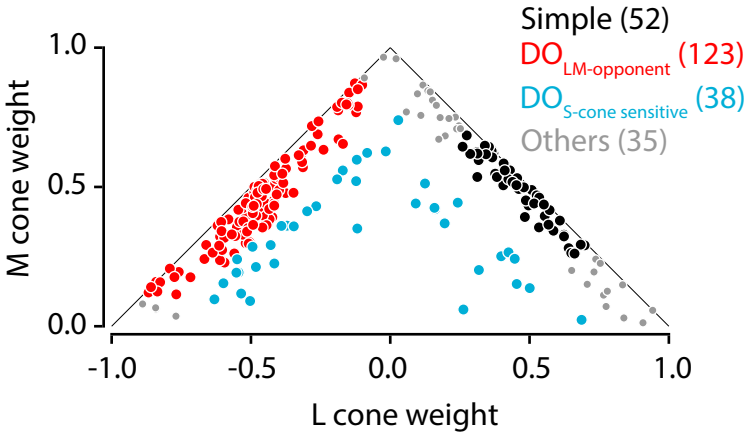

Figure S1. Reclassification of cells with reversed cone weight criteria. Shown are the normalized cone weights of simple (black), $DO_{LM\text{-}opponent}$ (red), $DO_{S\text{-}cone\ sensitive}$ (blue) and unclassified (gray) cells. M-cone weights were constrained to be positive. Cells were classified as simple if the L- and M-cone weights had the same sign, that together, accounted for 80% of the total cone weight and individually accounted for at least 30%. Cells were labeled as $DO_{LM\text{-}opponent}$ if the L- and M-cone weights had opposite sign, together accounted for 80% and individually accounted for at least 10% of the total cone weight. Classification of $DO_{S\text{-}cone\ sensitive}$ was same as the original as described in the Methods. The remaining cells were labeled as unclassified.

Figure S2

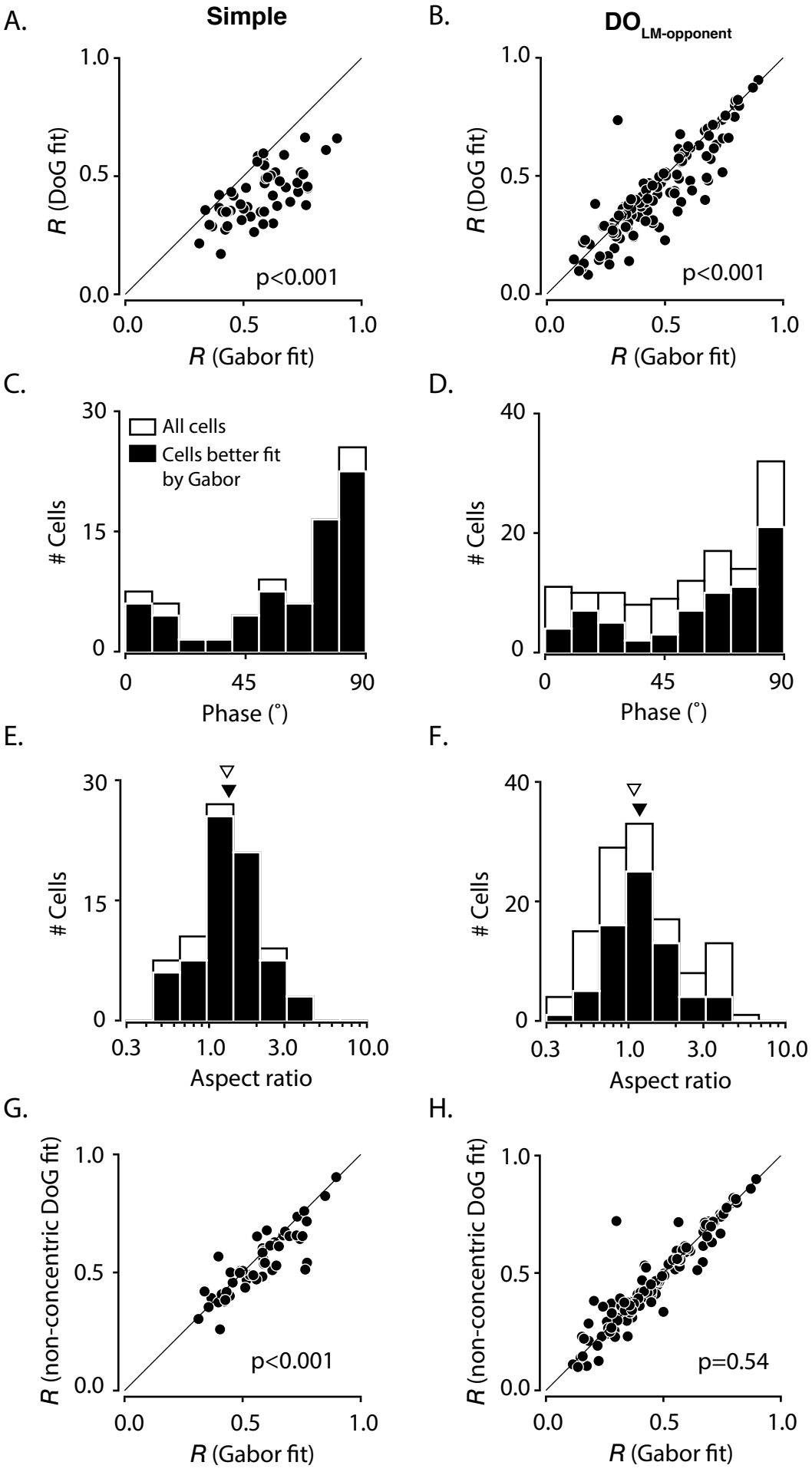

Figure S2. Model comparisons after reclassification of cells. **A.** Cross validated *R* from Gabor fit is plotted against DoG fit for simple cells. **B.** Identical to **A** but for $DO_{LM\text{-}opponent}$ cells. **C.** Analyses of best fitting phase (φ) of Gabor fits to all simple RFs (white) and those that are better fit by the Gabor model than the DoG model (black). The mean φ is 60.6° for simple RFs and 61.8° for cells better fit by Gabor model. **D.** Identical to **C** but for $DO_{LM\text{-}opponent}$ RFs. The mean φ is 55.0° for all $DO_{LM\text{-}opponent}$ RFs and 59.4° for cells better fit by Gabor model. **E.** Analyses of best fitting aspect ratio (γ) of Gabor fits to all simple RFs (white) and those that are better fit by the Gabor model than the DoG model (black). The median γ is 1.30 for all simple cell RFs and 1.34 for cells better fit by Gabor model. **F.** Identical to **E** but for DO RFs. The median γ is 1.09 for all simple cell RFs and 1.18 for cells better fit by Gabor model. **G.** Cross-validated *R* from Gabor fit is plotted against non-concentric DoG fit for simple cells. **H.** Identical to **G** but for $DO_{LM\text{-}opponent}$ cells.

Figure S3

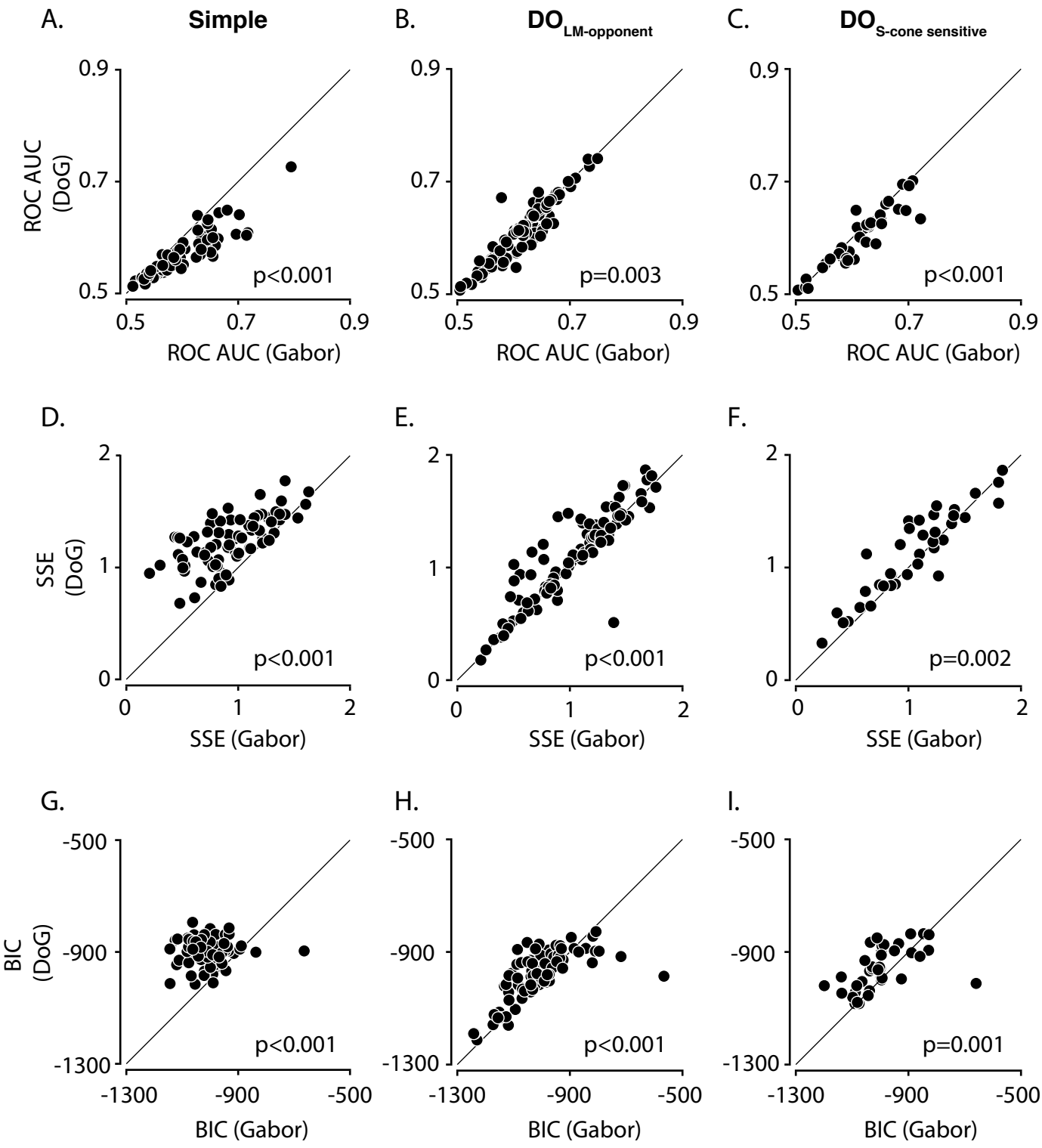

Figure S3. Comparison of Gabor and DoG model fits. Plotted are the results from three different analyses to compare model fits to the spatial RFs of simple, $DO_{LM\text{-}opponent}$ and $DO_{S\text{-}cone\ sensitive}$ cells. **A.** Cross validated spike predictability using receiver operating characteristics (ROC) from Gabor fits is plotted against the DoG fits for simple cells. **B.** Identical to **A.** but for $DO_{LM\text{-}opponent}$ cells **C.** Identical to **A.** but for $DO_{S\text{-}cone\ sensitive}$ cells. **D.** Cross validated sum of squared errors (SSE) from Gabor fits is plotted against the DoG fits for simple cells. E. Identical to **D.** but for $DO_{LM\text{-}opponent}$ cells. **F.** Identical to **D.** but for $DO_{S\text{-}cone\ sensitive}$ cells. **G.** Bayesian Information Criteria (BIC) from Gabor fits is plotted against the DoG fits for simple cells. A better model fit yields a lower BIC. **H.** Identical to **G.** but for $DO_{LM\text{-}opponent}$ cells. **I.** Identical to **G.** but for $DO_{S\text{-}cone\ sensitive}$ cells.

Figure S4

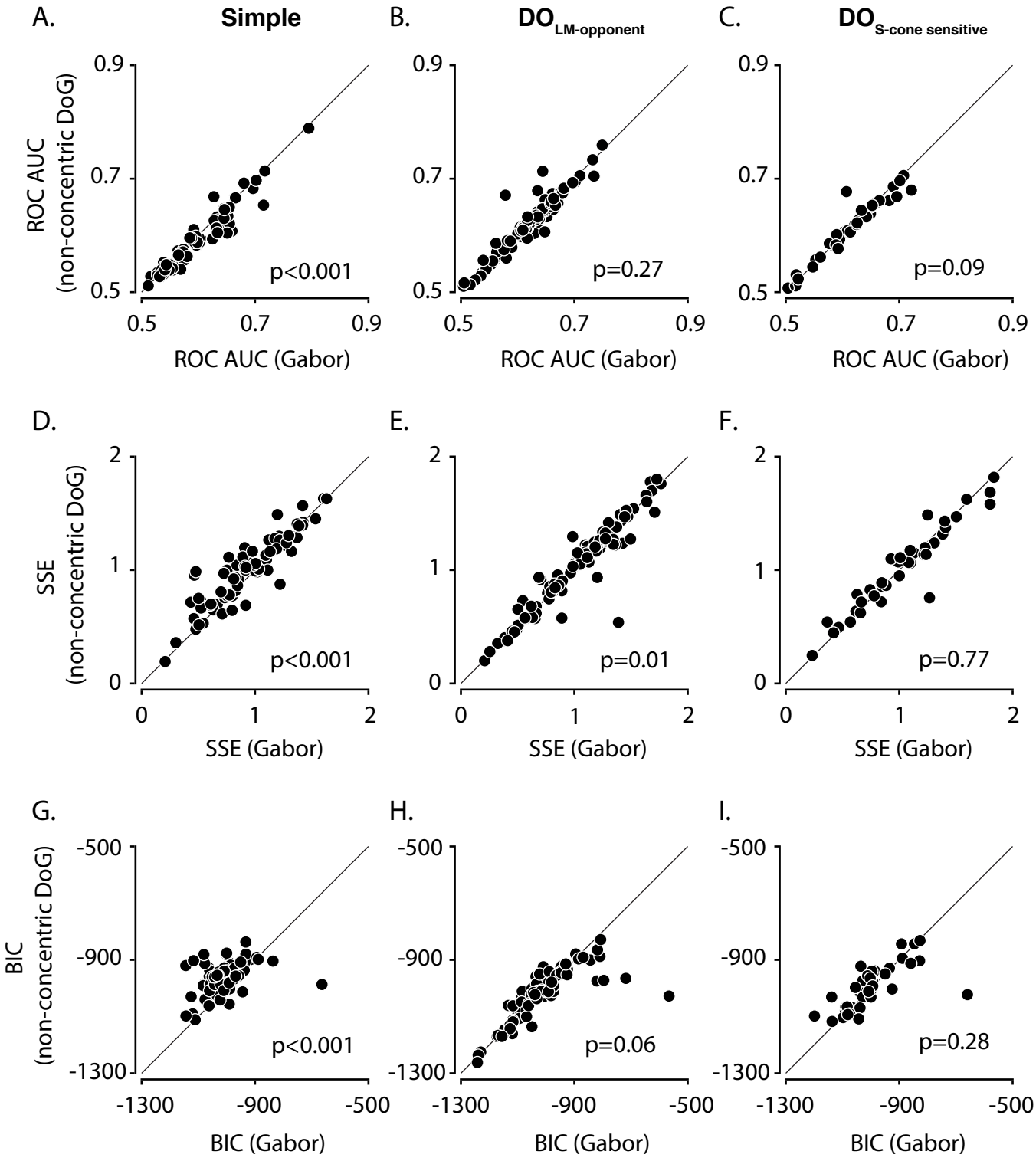

Figure S4. Comparison of Gabor and non-concentric DoG model fits. Plotted are the results from three different analyses to compare model fits to the spatial RFs of simple, $DO_{LM\text{-}opponent}$ and $DO_{S\text{-}cone\ sensitive}$ cells. **A.** Cross validated spike predictability using receiver operating characteristics (ROC) from Gabor fits is plotted against the non-concentric DoG fits for simple cells. **B.** Identical to **A.** but for $DO_{LM\text{-}opponent}$ cells. **C.** Identical to **A.** but for $DO_{S\text{-}cone\ sensitive}$ cells. **D.** Cross validated sum of squared errors (SSE) from Gabor fits is plotted against the non-concentric DoG fits for simple cells. **E.** Identical to **D.** but for $DO_{LM\text{-}opponent}$ cells. **F.** Identical to **D.** but for $DO_{S\text{-}cone\ sensitive}$ cells. **G.** Bayesian Information Criteria (BIC) from Gabor fits is plotted against the non-concentric DoG fits for simple cells. A better model fit yields a lower BIC. **H.** Identical to **G.** but for $DO_{LM\text{-}opponent}$ cells. **I.** Identical to **G.** but for $DO_{S\text{-}cone\ sensitive}$ cells.